

## Results of a modified PROMISE experiment

F. Stefani<sup>1,\*</sup>, G. Gerbeth<sup>1</sup>, Th. Gundrum<sup>1</sup>, J. Szklarski<sup>1</sup>, G. Rüdiger<sup>2</sup>, and R. Hollerbach<sup>3</sup>

<sup>1</sup> Forschungszentrum Dresden-Rossendorf, P.O. Box 510119, D-01314 Dresden, Germany

<sup>2</sup> Astrophysikalisches Institut Potsdam, An der Sternwarte 16, D-14482 Potsdam, Germany

<sup>3</sup> Department of Applied Mathematics, University of Leeds, Leeds LS2 9JT, UK

Received 2008 Jun 27, accepted 2008 Jun 30

Published online 2008 Aug 30

**Key words** magnetic fields – magnetohydrodynamics (MHD)

The PROMISE experiment relies on the fact that the critical Reynolds number for the appearance of the magnetorotational instability (MRI) in liquid metal flows drastically decreases when the purely axial magnetic field is replaced by a helical one. We report the results of a modified version of this experiments in which the radial electrical boundary conditions are changed. Special focus is laid on the role of the radial jet region where the two Ekman vortices from the top and the bottom meet each other.

© 2008 WILEY-VCH Verlag GmbH & Co. KGaA, Weinheim

### 1 Introduction

The magnetorotational instability (MRI) plays a key role in explaining turbulence and angular momentum transport in accretion disks. Its astrophysical importance had been considered in a seminal paper by Balbus & Hawley (1991) who showed that even weak magnetic fields can dramatically alter the stability criterion of rotating flows. However, the basic idea of MRI was not completely new since Velikhov (1959) and Chandrasekhar (1960) had demonstrated that an axial magnetic field could destabilize a Rayleigh-stable Taylor-Couette (TC) flow, provided the angular velocity decreases with radius.

If, in a TC flow, the ratio  $\mu := f_o/f_i$  of the outer and inner cylinders' rotation rates is less than the squared ratio  $(r_i/r_o)^2$  of the inner and outer cylinders' radii, then according to the Rayleigh criterion (Rayleigh 1929) the flow is always unstable, at least in the inviscid limit. In contrast, if  $\mu$  is greater than one, then according to the Velikhov-Chandrasekhar criterion the flow is stable, though even flows with positive shear can be magnetically destabilized by the Hall effect (Rüdiger & Shalybkov 2004). The relevant region for MRI lies between the Rayleigh line and the Velikhov-Chandrasekhar lines, where the angular momentum increases while the angular velocity decreases with radius. This is the regime where the flow is hydrodynamically stable (Ji et al. 2006), but magnetohydrodynamically unstable.

The last decade has witnessed growing interest in liquid metal experiments to investigate MRI in the laboratory (Rosner et al. 2004). For the classical Velikhov-Chandrasekhar-Balbus-Hawley configuration, with the externally applied magnetic field being purely axial, these at-

tempts have not entirely succeeded so far. The main problem with this “standard MRI” is that the azimuthal magnetic field, which is necessary for the MRI to proceed, must be *induced* from the applied axial field by the rotation of the flow. This is only possible in flows with sufficiently large magnetic Reynolds numbers  $R_m$ , which are difficult to achieve in the laboratory, typically only in sodium-cooled fast-breeder reactors or in special dynamo experiments (Gailitis et al. 2002). Sisan et al. (2004) had observed a coherent structure of velocity and magnetic field perturbations whose dependence on  $R_m$ , as well as on the field strength, is indeed rather similar to the classical MRI. This coherent structure arose from an already highly turbulent background flow, contradicting the original goal of identifying the MRI as the *first* instability on a laminar background flow. Nevertheless, it is tempting to speculate (in the spirit of Liu 1989) that the fine-grained background turbulence just results in a renormalized viscosity, without fundamentally affecting the basic mechanism of MRI that seems robust enough to show up as a “coherent structure” provided only  $R_m$  and the magnetic field strength are in the right range.

Considering this difficulty to produce the required azimuthal field by the flow, one could ask why not to replace the induction process by *externally applying* an azimuthal magnetic field as well? This question was addressed in a recent paper by Hollerbach & Rüdiger (2005), who showed that the MRI is then possible with dramatically reduced experimental effort. Actually, the scaling characteristics are completely different to those of “standard” MRI. While the latter needs magnetic Reynolds numbers  $R_m$  and Lundquist numbers  $Lu$  of the order of 1, the former depends on the hydrodynamical Reynolds number  $Re$  and the Hartmann number  $Ha$ .

This new type of MRI, sometimes called the “helical MRI” (HMRI) or the “inductionless MRI”, is currently the

\* Corresponding author: F.Stefani@fzd.de

subject of intense discussions in the literature (Szklański & Rüdiger 2006; Liu et al. 2006; Priede et al. 2007; Szklarski & Rüdiger 2007; Szklarski 2007; Liu et al. 2007; Liu 2008; Szklarski & Gerbeth 2008). The astrophysical relevance of magnetorotational instabilities in helical magnetic fields is still a matter of some controversy, dating back to an early dispute between Knobloch (1991) and Hawley & Balbus (1992). However, before entering such a discussion in detail, one has to check if HMRI works at all for Keplerian rotation profiles  $\Omega(r) \sim r^{-3/2}$ . While the answer resulting from the dispersion relation was negative (Liu et al. 2006), the solution of the eigenvalue equation gave an affirmative answer as long as at least the outer or the inner radial boundary is conducting (Rüdiger & Hollerbach 2007).

Unfortunately, even this is not the end of the story. Since HMRI appears in the form of a travelling wave (Knobloch 1996; Hollerbach & Rüdiger 2005), one has to be quite careful with the interpretation of instability of a single monochromatic wave. Actually, one has to look for wave packet solutions with vanishing group velocity. Typically, the regions in parameter space for this *absolute instability* are only a subset of the *convective instability*. A comprehensive analysis of this topic was presented recently by Gerbeth & Priede (2007).

Notwithstanding this ongoing discussion, the dramatic decrease of the critical Reynolds number for the onset of the MRI in helical magnetic fields, as compared with the case of a purely axial field, makes this new type of MRI very attractive for experimental studies. Results of the experiment “PROMISE” (Potsdam ROssendorf Magnetic InStability Experiment) were published recently (Stefani et al. 2006; Rüdiger et al. 2006; Stefani et al. 2007). Most important among them was the appearance of MRI in form of a travelling wave in a limited window of the magnetic field strength. The frequency of this wave turned out to be in good agreement with numerical predictions.

However, there are some intricacies in this first PROMISE experiment which trace back to the two points discussed above. First, the realm of HMRI only extends slightly beyond the Rayleigh line, and second, this small region for the convective instability is further reduced when focusing on the absolute instability. With view on this high sensitivity of the instability with respect to  $\mu := f_o/f_i$  one has to check carefully the effect of Ekman pumping at the end caps and also a possible change of the rotation profiles due to the interaction of Hartmann currents and the axial field which is able to drive a Dean flow (Szklański 2007; Priede 2007; Szklarski & Gerbeth 2008). A related issue is the critical role of the radial jet that appears approximately at mid-height of the Taylor-Couette cell (Kageyama 2004) and at which the MRI wave is typically stopped (Stefani et al. 2006). This radial jet results from the Ekman pumping at the lower and upper end caps, and can certainly be influenced by the Hartmann currents (Szklański 2008).

Although the most favorable way to minimize the Ekman pumping and thereby the radial jet is by the use of split

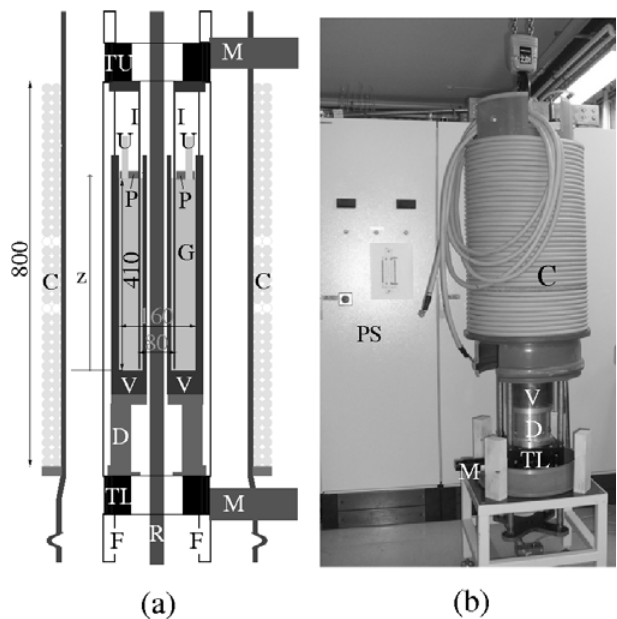


**Fig. 1** The complete PROMISE facility. (a) Schematic sketch, with the numbers indicating lengths in mm. (b) Photograph of the facility with the coil being installed. The letters denote the following: V – Copper vessel, I – Inner cylinder, G – GaInSn, U – Two ultrasonic transducers, P – Plexiglass lid, TL – Lower high precision turntable, TU – Upper high precision turntable, M – Motors, F – Frame, C – Coil, R – Copper rod, PS – Power supply up to 8000 A.

rings at the end caps of the TC cell (Szklański 2007), it is also of some interest to understand better the intricate interaction of Ekman pumping and the Hartmann current induced flow. For this reason we have decided to carry out a slightly modified version of the PROMISE experiment in which the radial electrical boundary conditions are changed. We do this by electrically insulating the inner cylinder, so that the Hartman currents are weakened. We will see in this paper how this simple modification changes the position of the radial jet with significant consequences for the fraction of the cylinder height in which the MRI wave can develop.

## 2 Experimental set-up

Figure 1 shows the PROMISE facility which consists basically of a cylindrical Taylor-Couette cell with externally imposed axial and azimuthal (i.e., helical) magnetic fields.

Its primary component is a cylindrical copper vessel V, fixed on a precision turntable TL via an aluminum spacer D. The inner wall of this vessel is 10 mm thick, extending in radius from 22 to 32 mm; the outer wall, which forms the outer cylinder of the TC cell, is 15 mm thick, extending from 80 to 95 mm. The inner cylinder of the TC cell is also made of copper, but is fixed on an upper turntable TU, from which it is immersed into the liquid metal from above. It is 4 mm thick, extending in radius from 36 to 40 mm, leaving a 4 mm gap between it and the inner wall of the containment

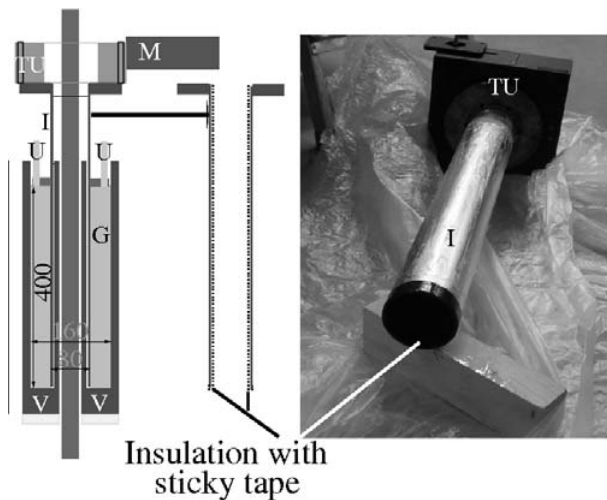


**Fig. 2** The change of radial boundary conditions by insulating the inner cylinder with sticky tape. Letters according to Fig. 1.

vessel V. The actual TC cell therefore extends in radius from 40 to 80 mm, for a gap width  $d = r_o - r_i = 40$  mm. This amounts to a radius ratio of  $\eta := r_i/r_o = 0.5$ . The fluid is filled to a height of 410 mm, for an aspect ratio of  $\sim 10$ .

Compared with the set-up documented in Stefani et al. (2006), Rüdiger et al (2006) and Stefani et al. (2007), we have modified the radial electrical boundary conditions by insulating the outer rim of the inner cylinder by sticky tape (Fig. 2). By this modification we intend to weaken the electric currents which are induced in the Hartmann layers and in the copper connection between innermost and outer cylinder (Szklański & Gerbeth 2008).

As working fluid we use the eutectic alloy  $\text{Ga}^{67}\text{In}^{20.5}\text{Sn}^{12.5}$ , which is liquid at room temperatures. The physical properties of GaInSn at 25 °C are as follows: density  $\rho = 6.36 \times 10^3 \text{ kg/m}^3$ , kinematic viscosity  $\nu = 3.40 \times 10^{-7} \text{ m}^2/\text{s}$ , electrical conductivity  $\sigma = 3.27 \times 10^6 (\Omega \text{ m})^{-1}$ . The magnetic Prandtl number is  $\text{Pm} = \mu_0 \sigma \nu = 1.40 \times 10^{-6}$ .

Note that the axial boundary conditions have not been changed. They are still asymmetric, both in the hydrodynamic and electric sense, with the upper plexiglass end plate being fixed to the frame F, and a lower endplate which is simply part of the copper vessel V, and thus rotates with the outer cylinder.

Note also that the use of copper cylinders compromises the obtainable geometrical accuracy of the experiment. Usually, in hydrodynamic TC experiments glass cylinders are used, which allow for very good geometrical accuracy, to within  $\sim 10^{-2}$  mm (Schultz-Grunow 1959). The use of copper cylinders was motivated by the fact that the critical Reynolds and Hartmann numbers for the onset of the MRI are somewhat smaller with perfectly conducting boundaries than with insulating boundaries (Rüdiger et al. 2005). The price to pay for this is that  $\sim 10^{-2}$  mm accuracy is no longer achievable when drilling and polishing a material as soft

as copper. What is more, to ensure a well-defined electrical contact between the fluid and the walls, it is necessary to intensively rub the GaInSn into the copper; the resulting abrasion then limits the accuracy to no better than  $\sim 10^{-1}$  mm.

The rotation frequencies of the inner and outer cylinders are measured by the Reynolds number  $\text{Re} = 2\pi f_i r_i d/\nu$  and the ratio  $\mu = f_o/f_i$ . Typical Reynolds numbers in the experiment are of  $O(10^3)$ , some 30 times greater than the  $\text{Re}_c = 68.2$  onset of nonmagnetic Taylor vortices in TC flows with  $\mu = 0$  (for a radius ratio  $\eta := r_i/r_o$  of 0.5, see (Chandrasekhar 1981). In our case with  $\eta = 0.5$ , the flow is Rayleigh-unstable for  $\mu < 0.25$  and Rayleigh-stable for  $\mu > 0.25$ .

We can independently apply axial and azimuthal magnetic fields. Axial magnetic fields of order 10 mT are produced by a double-layer coil (C). Currents up to 200 A are driven through this coil, achieving axial fields up to  $B_z = 20.35$  mT, or in nondimensional units up to a Hartmann number  $\text{Ha} := B_z(r_i d \sigma / \rho \nu)^{1/2}$  of 31.65. The azimuthal field  $B_\varphi$ , also of order 10 mT (at  $r_i$ ), is generated by a current through a water-cooled copper rod (R) of radius 15 mm. The power supply for this axial current delivers up to 8000 A. In the following this current will be referred to as the “rod current”. The ratio of azimuthal to axial field is measured by the parameter  $\beta := B_\varphi(r_i)/B_z$ .

Our measuring instrumentation consists exclusively of two ultrasonic transducers, fixed into the upper plexiglass lid, 15 mm away from the outer copper wall, flush mounted at the interface to the GaInSn, and with special high-focus sensors having a working frequency of 4 MHz. With this instrumentation we can then measure the axial velocity  $v_z$  at the particular location  $r = 65$  mm (averaged over the approximately 8 mm width of the ultrasound beam), as a function of time  $t$  and height  $z$  along the cylinder axis. The resolutions in  $t$  and  $z$  were adjustable (within limits); in most runs we used resolutions of 1.84 s in  $t$  and 0.685 mm in  $z$ . Finally, having two transducers, on opposite sides of the TC cell, was important in order to be able to distinguish between the expected axisymmetric ( $m = 0$ ) MRI, and an unexpected non-axisymmetric  $m = 1$  instability which was already observed in Stefani et al. (2007) and will also be discussed below.

### 3 Results

In this section we will present the results of the modified PROMISE experiment. We start with Fig. 3, showing the difference in the upward travelling MRI wave between the old experiment (Fig. 3a) with non-insulated inner cylinder (which will be abbreviated by NIIC in the following) and the new experiment (Fig. 3b) with insulated inner cylinder (IIC). The physical parameters in this case are  $f_i = 0.06$  Hz,  $f_o = 0.0162$  Hz,  $I_{\text{coil}} = 60$  A,  $I_{\text{rod}} = 6000$  A, which corresponds to the dimensionless parameters  $\text{Re} = 1775$ ,  $\mu = 0.27$ ,  $\text{Ha} = 9.49$ ,  $\beta = 4.92$ . The grayscale indicates

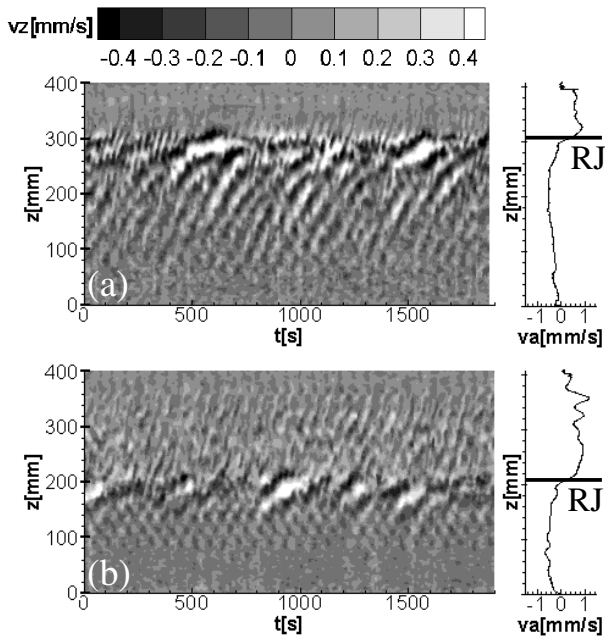


**Fig. 3** Upward travelling MRI wave, (a) in the experiment with non-insulated inner cylinder (NIIC), and (b) with insulated inner cylinder (IIC).

the perturbation of the axial velocity component measured along the ultrasound beam, in dependence on the time  $t$  and the vertical position  $z$ . The velocity perturbation has been obtained by subtracting from the measured signal the time averaged axial velocity  $va(z)$ , which is shown in the separate graph on the right-hand side of the plots.

These graphs are very instructive since they show a rather sharp transition between positive and negative mean axial velocity indicating (by virtue of the continuity condition) the existence of a rather sharp radial jet (RJ). The interesting thing is now that the position of this radial jet differs strongly between the NIIC and the IIC setting. While for NIIC it is approximately at 3/4 of the total height, it moves to approximately mid height in the ICC case. This position of the radial jet has a remarkable effect on the behaviour of the MRI wave. As already observed earlier (Stefani et al. 2006; Stefani et al. 2007), the MRI wave develops and continues only up to the radial jet position, where it is stopped. It is evident that in the IIC case this fraction is much smaller so that the MRI wave can not develop properly.

In Fig. 4 we show the corresponding results for the downward travelling MRI wave which appears when the sign of  $B_z$  was changed (actually, the direction of propagation, i.e. whether the pattern drifts in the  $+z$  or  $-z$  direction, depends on whether the screw sense of the magnetic field is either anti-parallel or parallel to the flow rotation). Again we see the different fractions of the height in which the MRI wave can develop. However, in the NIIC case the sharp transition between positive and negative axial velocities is replaced by a rather smooth transition which makes the identification of a radial jet difficult. Contrary to this,

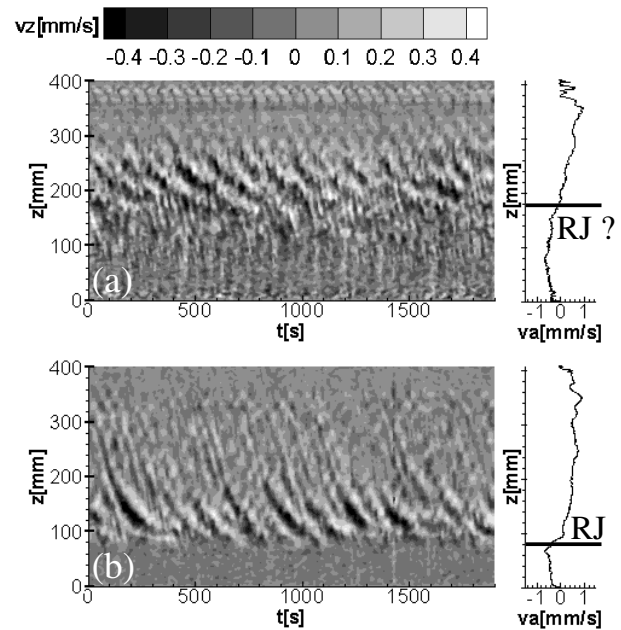


**Fig. 4** Downward travelling MRI wave, (a) in the experiment with non-insulated inner cylinder (NIIC), and (b) with insulated inner cylinder (IIC).

the radial jet in the ICC case is well expressed and sits at approximately 1/5 of the total height, so that the MRI wave has a rather long way to develop.

One of the unexpected results of the PROMISE experiment was the detection of a non-axisymmetric ( $m = 1$ ) mode in certain parameter regions (Stefani et al. 2007). The typical frequency of this mode is approximately one half of  $f_i$ , in contrast to the basic MRI mode, which has typical frequencies of 0.1–0.2 of  $f_i$ . The origin of this  $m = 1$  mode is not clear yet. A possible source of it could be the fact that the apparatus is not perfectly symmetric. In particular, the leads that feed the rod current induce a non-axisymmetric field component which requires further numerical simulations.

Focusing in the following exclusively on the IIC case, we will present some results which might be helpful in understanding the  $m = 1$  mode. Figure 5 shows the downward travelling mode, with the following parameters:  $f_i = 0.02 \dots 0.05$  Hz,  $f_o = 0.0054 \dots 0.0135$  Hz,  $I_{\text{coil}} = 60$  A,  $I_{\text{rod}} = 7320$  A, corresponding to the dimensionless parameters  $Re = 592 \dots 1479$ ,  $\mu = 0.27$ ,  $Ha = 9.49$ ,  $\beta = 6.0$ .

Although the wave pattern that appears for  $f_i = 0.02$  Hz and  $f_i = 0.03$  Hz, looks like a MRI wave, on closer inspection (comparison of the signals from the two sensors at opposite azimuths) it turns out to be a  $m = 1$  mode, with a frequency of approximately  $0.5 f_i$ . However, it is most interesting to see that this mode is replaced by the proper  $m = 0$  MRI wave for  $f_i = 0.04$  Hz and  $f_i = 0.05$  Hz, with a frequency that is approximately  $0.2 f_i$ .

The corresponding case with an upward travelling wave is particularly interesting. In Fig. 6 we see that an  $m = 1$  wave appears first, but this time it starts at the radial jet

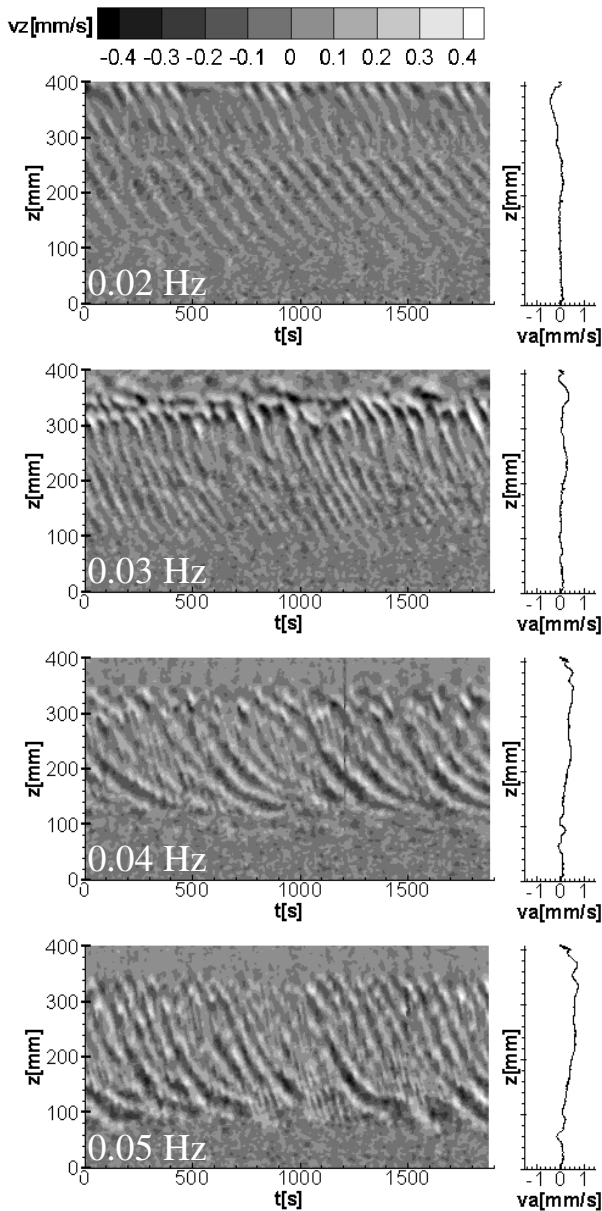


**Fig. 5** Downward travelling wave for varying  $f_i$  (i.e. Re number). For  $f_i = 0.02$  Hz and  $f_i = 0.03$  Hz the  $m = 1$  mode dominates, for  $f_i = 0.04$  Hz and  $f_i = 0.05$  Hz the  $m = 0$  MRI wave comes up.

position and travels to the upper end cap. In the lower region between the bottom and the radial jet position, the  $m = 0$  MRI wave comes up for higher Re and coexists with the  $m = 1$  wave in the upper part.

In the last two figures we document the dependence of the MRI wave on the current in the coil which is proportional to the Hartmann number (in our case we have  $Ha = 0.158 \times I_{\text{coil}}/A$ ). In both cases, the parameters are as follows:  $f_i = 0.06$  Hz,  $f_o = 0.0162$  Hz,  $I_{\text{coil}} = 0 \dots 120$  A,  $I_{\text{rod}} = 6000$  A, corresponding to the dimensionless parameters  $Re = 1775$ ,  $\mu = 0.27$ ,  $Ha = 0 \dots 18.96$ ,  $\beta = \infty \dots 2.46$ .

In Fig. 7 we show the case of the upward travelling wave, which we already know from Fig. 3b to have only

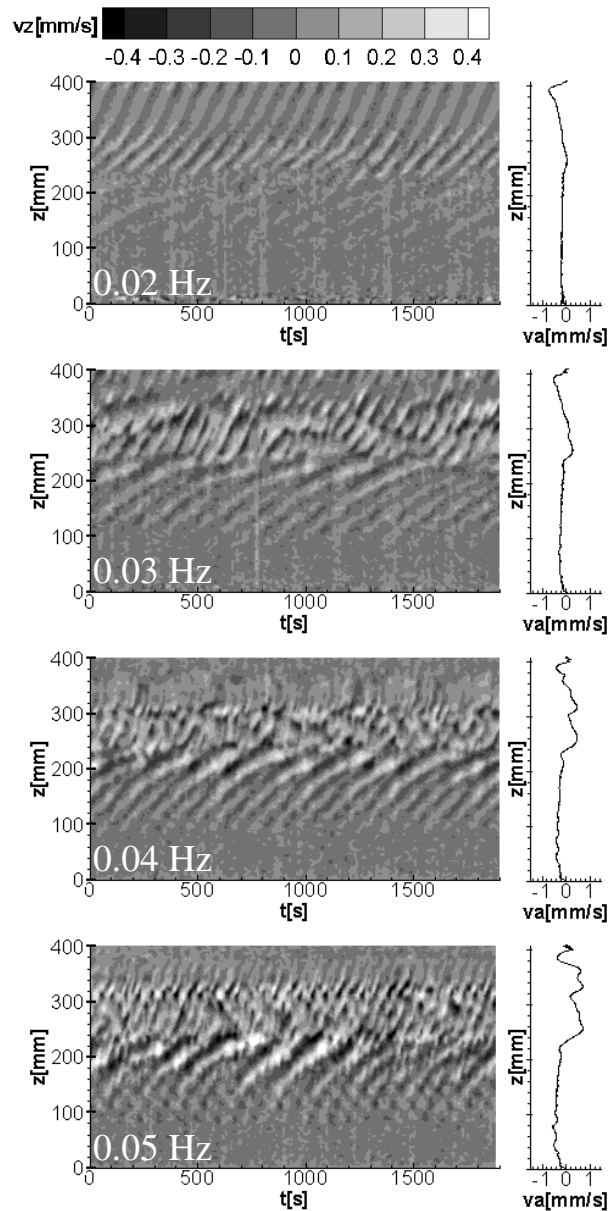


**Fig. 6** Upward travelling MRI wave, for varying  $f_i$  (i.e. Re number). For  $f_i = 0.02$  Hz and  $f_i = 0.03$  Hz  $m = 1$  mode dominates in the upper part of the TC cell, for  $f_i = 0.04$  Hz and  $f_i = 0.05$  Hz the  $m = 0$  MRI wave comes up in the lower part.

half the height of the cylinder to develop until it is stopped by the radial jet. Despite this restriction, we see a similar window of the appearance of the wave as in Stefani et al. (2006).

In contrast, the downward travelling wave (Fig. 8) has more space to develop, and fills the cylinder from the top to approximately 1/5 above the bottom.

## 4 Conclusions

After the existence of MRI waves, and their expected appearance in a finite window of the Hartmann number had

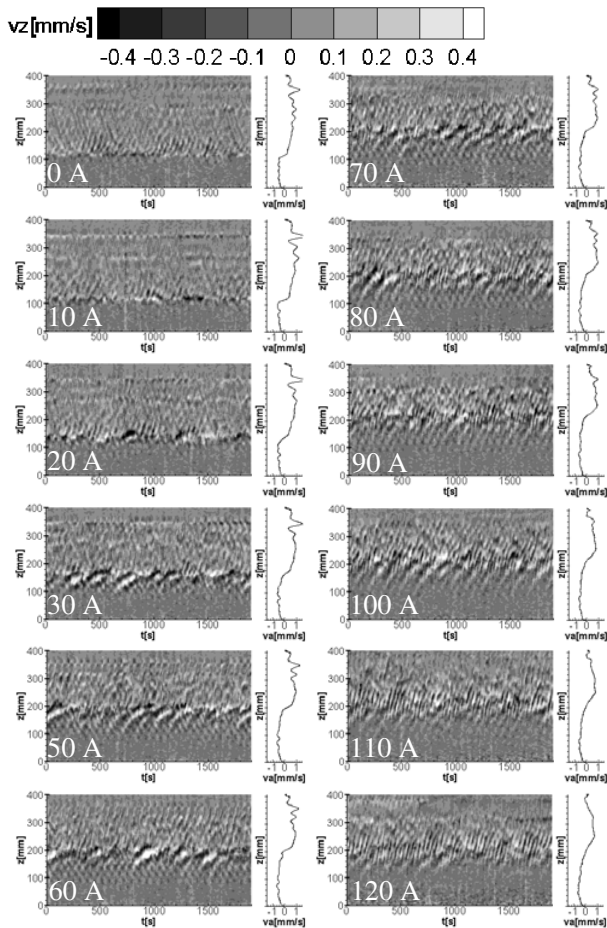


Fig. 7 Upward travelling MRI wave, for varying  $I_{\text{coil}}$ .

been demonstrated in a number of papers (Stefani et al. 2006; Rüdiger et al. 2006; Stefani et al. 2007), we have presented in this paper some additional results from complementary measurements of a PROMISE experiment with modified radial boundary conditions. We have made clear that the radial jet, resulting from the non-symmetric Ekman pumping and the Hartmann currents, plays a significant role in restricting the height in which the MRI wave can develop. We have documented the transition between  $m = 1$  and  $m = 0$  modes for increasing Reynolds number, and partly the coexistence of both modes in the two regions separated by the radial jet.

Besides the fact that a better numerical understanding of the complex interaction of Ekman pumping and Hartmann currents is certainly elusive, the main lesson to learn from this experiment is that it is essential to minimize the Ekman pumping in order to get clearer results. Such experiments have already been done, and will be documented elsewhere.

*Acknowledgements.* This work was supported by the German Leibniz Gemeinschaft, within its Senatsausschuss Wettbewerb (SAW) programme.

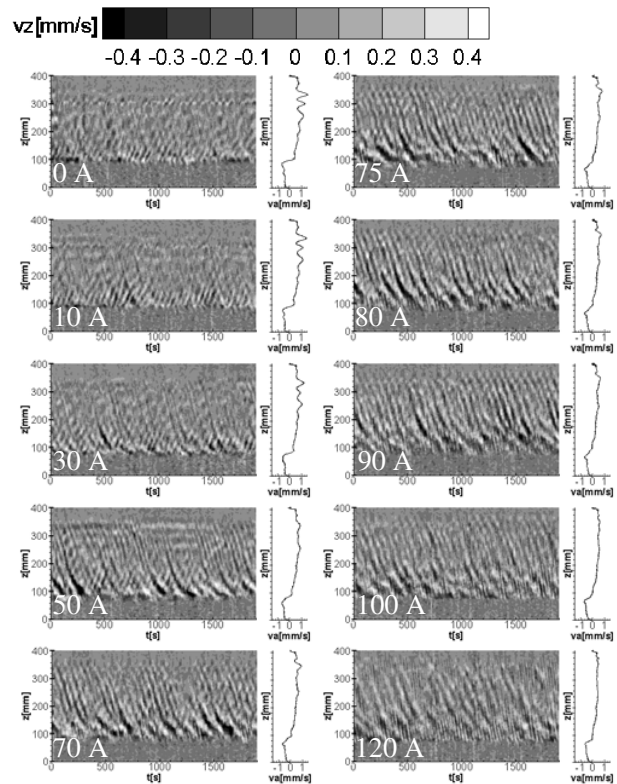


Fig. 8 Downward travelling MRI wave, for varying  $I_{\text{coil}}$ .

## References

- Balbus, S.A., Hawley, J.F.: 1991, *ApJ* 376, 214  
 Chandrasekhar, S.: 1960, *Proc. Nat. Acad. Sci.* 46, 253  
 Chandrasekhar, S.: 1981, *Hydrodynamic and Hydromagnetic Instability*, Dover, New York, p. 323  
 Gailitis, A., Lielausis, O., Platācis, E., Gerbeth, G., Stefani, F.: 2002, *RVMP* 74, 973  
 Gerbeth, G., Priede, J.: 2007, Absolute vs. convective helical MRI in a TC flow, Presentation at the MRI workshop, Catania, 1-3 October 2007  
 Hawley, J.F., Balbus, S.A.: 1992 *ApJ* 400, 595  
 Hollerbach, R., Rüdiger, G.: 2005, *Phys Rev Lett* 95, 124501  
 Ji, H., Burin, M., Schartman, E., Goodman, J.: 2006, *Nature* 444, 343  
 Kageyama, A., Ji, H., Goodman, J., Chen, F., Shoshan, E.: 2004, *J. Phys. Soc. Jpn.* 73, 2424  
 Knobloch, E.: 1991, *MNRAS*, 255, 25  
 Knobloch, E.: 1996, *PhFl* 8, 1446  
 Liu, J.T.C.: 1989, *AnRFM* 21, 285  
 Liu, W., Goodman, J., Ji, H.: 2007, *Phys Rev E* 76, 016310  
 Liu, W., Goodman, J., Herron, I., Ji, H.: 2006, *Phys Rev E* 74, 056302  
 Priede, J.: 2007, Pseudo magnetorotational instability in a TC flow between electrically connected cylinders, Presentation at the MRI workshop, Catania, 1-3 October 2007  
 Priede, J., Grants, I., Gerbeth, G.: 2007, *Phys Rev E* 75, 047303  
 Rayleigh Lord: 1929, On the dynamics of revolving fluids, *Scientific papers* 6, 447  
 Rosner, R., Rüdiger, G., Bonanno, A.: 2004, *MHD Couette Flows: Experiments and Models*, American Institute of Physics Melville, New York

- Rüdiger, R., Hollerbach, G.: 2007, Phys Rev E 76, 068301
- Rüdiger, G., Hollerbach, R., Schultz, M., Shalybkov, D.A.: 2005, AN 326, 409
- Rüdiger, G., Hollerbach, R., Stefani, F., Gundrum, T., Gerbeth, G., Rosner, R.: 2006, ApJ 649, L145
- Schultz-Grunow, F.: 1959, ZaMM 39, 101
- Sisan, D.R., Mujica, N., Tillotson, W.A., Huang, Y.-M., Dorland, W., Hassam, A.B., Antonsen, T.M., Lathrop, D.P.: 2004, Phys Rev Lett 93, 114502
- Stefani, F., Gundrum, T., Gerbeth, G., Rüdiger, G., Schultz, M., Szklarski, J., Hollerbach, R.: 2006, Phys Rev Lett 97, 184502
- Stefani, F., Gundrum, T., Gerbeth, G., Rüdiger, G., Szklarski, J., Hollerbach, R.: 2007, NJPh 9, 295
- Szklarski, J.: 2007, AN 328, 499
- Szklarski, J., Gerbeth, G.: 2008, AN 329, 667
- Szklarski, J., Rüdiger, G.: 2006, AN 327, 844
- Szklarski, J., Rüdiger, G.: 2007, Phys Rev E 76, 066308
- Velikhov, E.P.: 1959, SJETP 36, 1398